

Kinematics and surface fracture pattern of the Anaran basement fault zone in NW of the Zagros fold–thrust belt

M. Joudaki¹ · A. Farzipour-Saein¹ · F. Nilfouroushan²

Received: 14 February 2015 / Accepted: 28 May 2015 / Published online: 11 June 2015
© Springer-Verlag Berlin Heidelberg 2015

Abstract The preexisting north–south trending basement faults and their reactivation played an important role during the evolution of the Zagros fold–thrust belt. The Anaran Basement Fault (ABF) in the Lurestan region, NW of the Zagros, has been considered as a N–S trending basement lineament, although its surface structural expression is still debated. In this study, we use satellite images and field observations to identify and analyze the fractures in the sedimentary cover above the ABF. Fracture analysis demonstrates that approaching the ABF, the fracture pattern changes. The fractures association with reactivation of the deep-seated preexisting ABF can be categorized in four sets based on their directions. The mean direction for maximum compressional stress is different between the fault- and fold-related fractures within and around the ABF shear zone. We estimated an orientation of $N30^\circ \pm 5^\circ$ for the fault-related fractures and $N45^\circ \pm 5^\circ$ for the fold-related fracture sets outside of the ABF shear zone. This difference suggests that the fold-related and fault-related fracture sets have been formed in different two stages of deformation throughout the area. The axial traces of some folds, especially the Anaran anticline, demonstrate a right-lateral offset along the ABF, such that, in central part of the Anaran anticline, the fold axis of this anticline is changed from its original NW–SE trend to approximately north–south trend of the ABF.

Keywords Anaran Basement Fault · Zagros · Remote sensing · Crustal deformation · Fracture analysis

Introduction

The Zagros fold–thrust belt (ZFTB) extends for about 1800 km through Iraq and Iran (Fig. 1) and formed due to continent–continent collision between African–Arabian plate and Iranian block (Takin 1972; Stöcklin 1974; Berberian and King 1981; Koyi 1988). This continental collision has made significant crustal shortening in the ZFTB and consequently caused cover and basement folding and faulting (Berberian 1995; Hessami et al. 2001a; Blanc et al. 2003; Nilfouroushan et al. 2003; McQuarrie 2004; Sepehr and Cosgrove 2005; Alavi 2007; Mouthereau et al. 2007a). The ZFTB hosts more than half of the world’s hydrocarbon reserves (Sepehr and Cosgrove 2005). High productivity of these reserves is related to the presence of fractures that have led to secondary effective porosity in carbonate reservoirs (Gholipour 1998; Ahmadhadi et al. 2008; Mobasher and Babaie 2008; Khoshbakht et al. 2009, 2012).

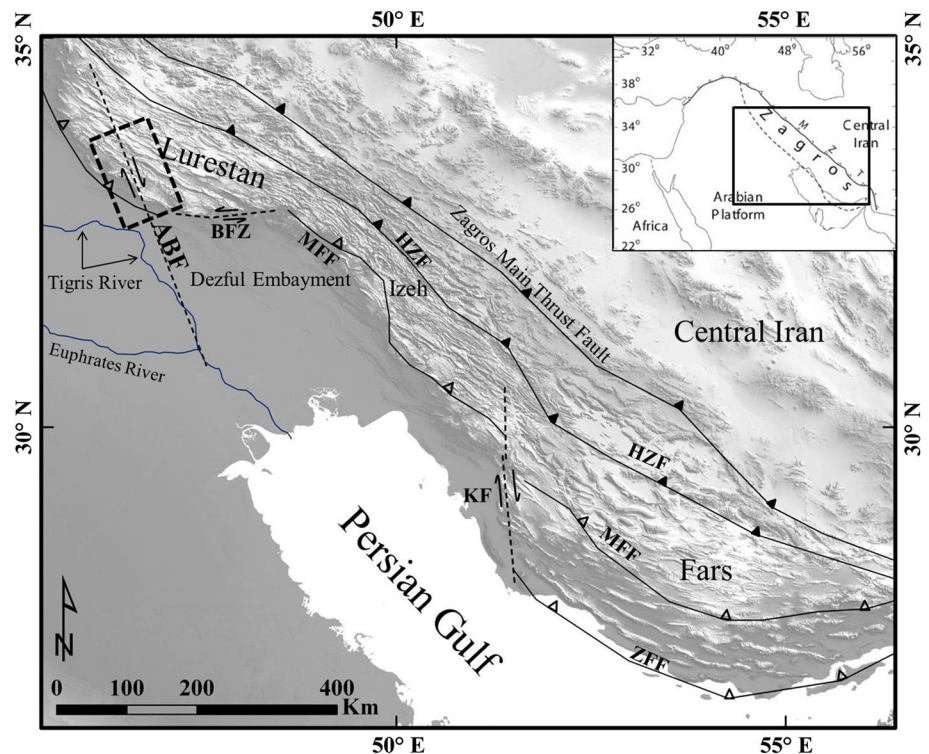
The orientation and intensity of fractures are typically related to macrostructures, such as folds, developing during progressive deformation of a sedimentary basin in Cenozoic (Anastasio et al. 1997; Storti and Salvini 2001; Bellahsen et al. 2006; Tavani et al. 2006; Mobasher and Babaie 2008; Amrouch et al. 2010; Lacombe et al. 2011; Tavani et al. 2015). In agreement, in the ZFTB, several sets of folding-related fractures have been recognized (McQuillan 1973, 1974; Gholipour 1998; Ahmadhadi et al. 2007; Mobasher and Babaie 2008; Lacombe et al. 2011). Indeed, other fracture systems oriented oblique to the trend of thrusts and folds are widely documented in the Zagros (e.g., McQuillan 1974; Carminati et al. 2013).

✉ A. Farzipour-Saein
asaein@gmail.com

¹ Department of Geology, University of Isfahan, P.O. Code: 81746-73441 Isfahan, Iran

² Department of Earth Sciences, Uppsala University, Villavägen 16, 752 36 Uppsala, Sweden

Fig. 1 Relief and simplified structural map of the Zagros fold–thrust belt shows the major structures of the Zagros and the location of the study area. *BFZ* Balarud Fault Zone, *ABF* Anaran Basement Fault, *HZF* High Zagros Fault, *KF* Kazerun Fault, *MFF* Mountain Front Fault, *ZFF* Zagros Front Fault



These oblique sets include fractures striking about N–S and E–W (e.g., Amrouch et al. 2010; Lacombe et al. 2011), and they have been interpreted as related with the reactivation of inherited, N–S striking, basement faults (e.g., Stephenson et al. 2007; Tavani et al. 2011). On the other hand, occurrence and reactivation of oblique inherited faults during thrusting, can determine local perturbation of the stress field and the development of local fracture patterns. Therefore, the study of fracture patterns can greatly help in individuating buried inherited fault systems. The activity of preexisting north–south trending basement faults and their effect on structural and sedimentation history in the ZFTB have been documented (Berberian 1995; Hessami et al. 2001a; Bahroudi and Talbot 2003; Sepehr and Cosgrove 2005; Ahmadhadi et al. 2007; Farzipour-Saein et al. 2009a, 2013). While the spatial density and dispersal variation of fold-related fractures depend on the fold geometry, a fault-related fracture system is localized along isolated linear zones, possibly marking boundaries of a basement block (Stephenson et al. 2007; Ahmadhadi et al. 2008; Lacombe et al. 2011).

In the ZFTB, fracture studies were mainly reported from the Dezful Embayment or the Fars region (Authemayou et al. 2006; Wennberg et al. 2006; Ahmadhadi et al. 2008; Mobasher and Babaie 2008; Khoshbakht et al. 2009; Lacombe et al. 2011; Khoshbakht et al. 2012). Some studies focused on fractures within single anticlines (McQuillan 1973, 1974; Wennberg et al. 2006; Stephenson et al. 2007), while others investigated fracture sets from a regional

view (Ahmadhadi et al. 2008; Mobasher and Babaie 2008; Lacombe et al. 2011).

The relationship between large geological structures and fractures in the cover and basement can more effectively be identified and studied through remote sensing technique (Stephenson et al. 2007; Mobasher and Babaie 2008; Casini et al. 2011; Snidero et al. 2011). In this study, we similarly used satellite images and field observations to study and analyze the distribution of fractures and their kinematics throughout the Anaran, Anjir, Kabir Kuh, Surgah, Ilam, A1 and A2 anticlines above the proposed Anaran basement lineament (Fig. 2). Although the Anaran Basement Fault (ABF) has been considered as N–S trending lineament (Farzipour-Saein et al. 2009a), its surface structural expression is still debated (Figs. 1, 2).

Regional geology

The Zagros Basin was part of the stable supercontinent of Gondwana in Paleozoic, a passive margin in Mesozoic and became a convergent orogeny in Cenozoic (Stocklin 1968; Berberian and King 1981; Berberian 1995; Agard et al. 2011; Mouthereau et al. 2012; McQuarrie and van Hinsbergen 2013). The NW–SE trending ZFTB is divided into three parallel structural and stratigraphic regions (Fig. 1), including the Foredeep, the Simply Folded Zone and the Imbricate Zone (Stocklin 1968; Falcon 1974; Berberian 1995; Sepehr and Cosgrove 2004).

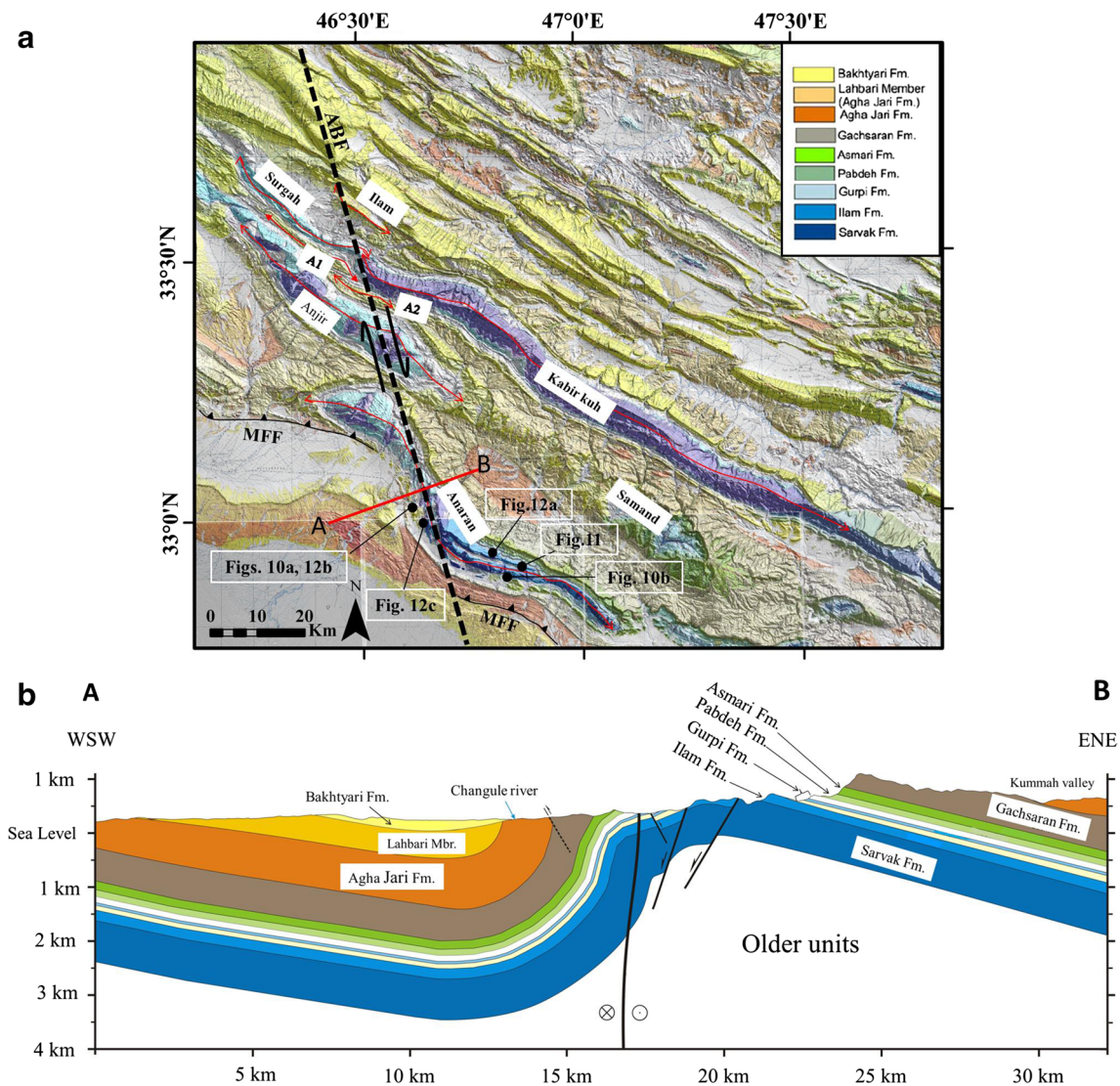


Fig. 2 **a** Geological map overlaid on the digital elevation model of the study area showing the main structures and formations. The Anaran Basement Fault (ABF) is marked by a *dashed line* (geologi-

cal map from NIOC). *Red line* across the Anaran anticline shows the position of the cross-section A, B. **b** Structural transect across the Anaran Basement Fault and the Anaran anticline

Recent studies (Talbot and Alavi 1996; Bahroudi and Talbot 2003; Bahroudi and Koyi 2004; Sherkati and Letouzey 2004; Farzipour-Saein et al. 2009a) show that the geometry of the Zagros deformation front and evolving foreland basin has been controlled by at least two different structural parameters: (1) reactivation of basement faults (Hessami et al. 2001a; Bahroudi and Talbot 2003; Sepehr and Cosgrove 2005; Ahmadi et al. 2007; Mouthereau et al. 2007a, b; Farzipour-Saein et al. 2009a; Nilfouroushan et al. 2013; Burberry 2015) and (2) mechanical nature of the sedimentary layers in the ZFTB (Bahroudi and Koyi 2003; Sherkati and Letouzey 2004; Farzipour-Saein et al. 2009b). Different evidences indicate that many of the transverse basement faults involve right-lateral strike-slip

displacements with dip-slip components (Baker et al. 1993; Berberian 1995; Hessami et al. 2001b; Bahroudi and Talbot 2003; Sepehr and Cosgrove 2005; Ahmadi et al. 2007; Farzipour-Saein et al. 2009a; Allen 2010).

In addition to orogeny-parallel zonation, based on structural features, the Simply Folded Zone can also be divided (along strike from east to west) into the Fars, Izeh, Dezful Embayment, Lurestan and Kirkuk Embayment (Sepehr and Cosgrove 2004; Sherkati and Letouzey 2004; Fig. 1). The Lurestan region (Fig. 1) has a long history of hydrocarbon exploration and production (Farzipour-Saein et al. 2009b). Stratigraphy of the Lurestan region consists of 10- to 12-km-thick succession that encompasses the Paleozoic and Mesozoic Arabian passive margin deposits, followed

by the sediments corresponding to the long-lived Cenozoic Zagros foreland infilling (Homke et al. 2004; Emami 2008; Farzipour-Saein et al. 2009b; Sharp et al. 2010; Vergés et al. 2011; Fig. 3). Two distinct folding patterns

(polyharmonic pattern in South and disharmonic pattern in North) can be observed in different parts of the Lurestan region (Farzipour-Saein et al. 2009b).

Photogeology studies and field observations in north-western part of the Lurestan demonstrate some N–S trending lineaments that cut NW–SE trending anticlines (Player et al. 1966; Motiei 1994). North–south trending basement faults have played an important role in basin evolution in the Lurestan region (Farzipour-Saein et al. 2009a). Farzipour-Saein et al. (2009a), based on sedimentary isopach maps and gravity data (Fig. 4), investigated the foreland basin history in the Lurestan region. They have expressed the Zagros orogeny together with activity of the preexisting north–south trending basement faults on foreland basin evolution in the Lurestan region. They proposed that during deposition of Cenomanian and Oligocene–Miocene sediments in south of the Lurestan, the architecture of the foreland basin was influenced by the deep-seated, approximately north–south trending, Anaran lineament. During Cenomanian to early Miocene time interval, this lineament was reactivated to form a paleohigh in southern part of the Lurestan region (Farzipour-Saein et al. 2009a).

The geometry and structural evolution of the Anaran anticline as a fault-related fold and its relationships to

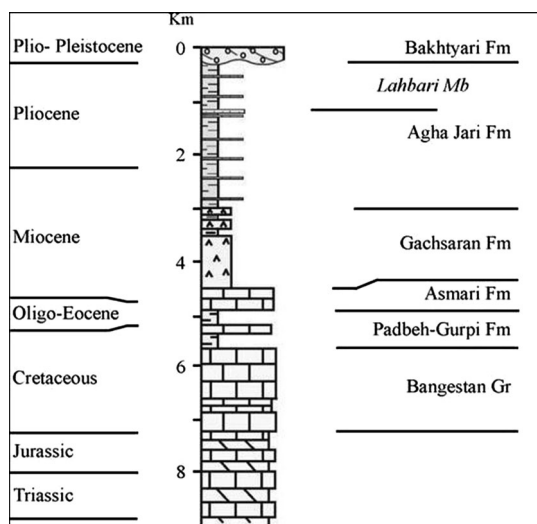


Fig. 3 Schematic stratigraphic column of the sedimentary cover of the Lurestan region (after Homke et al. 2004)

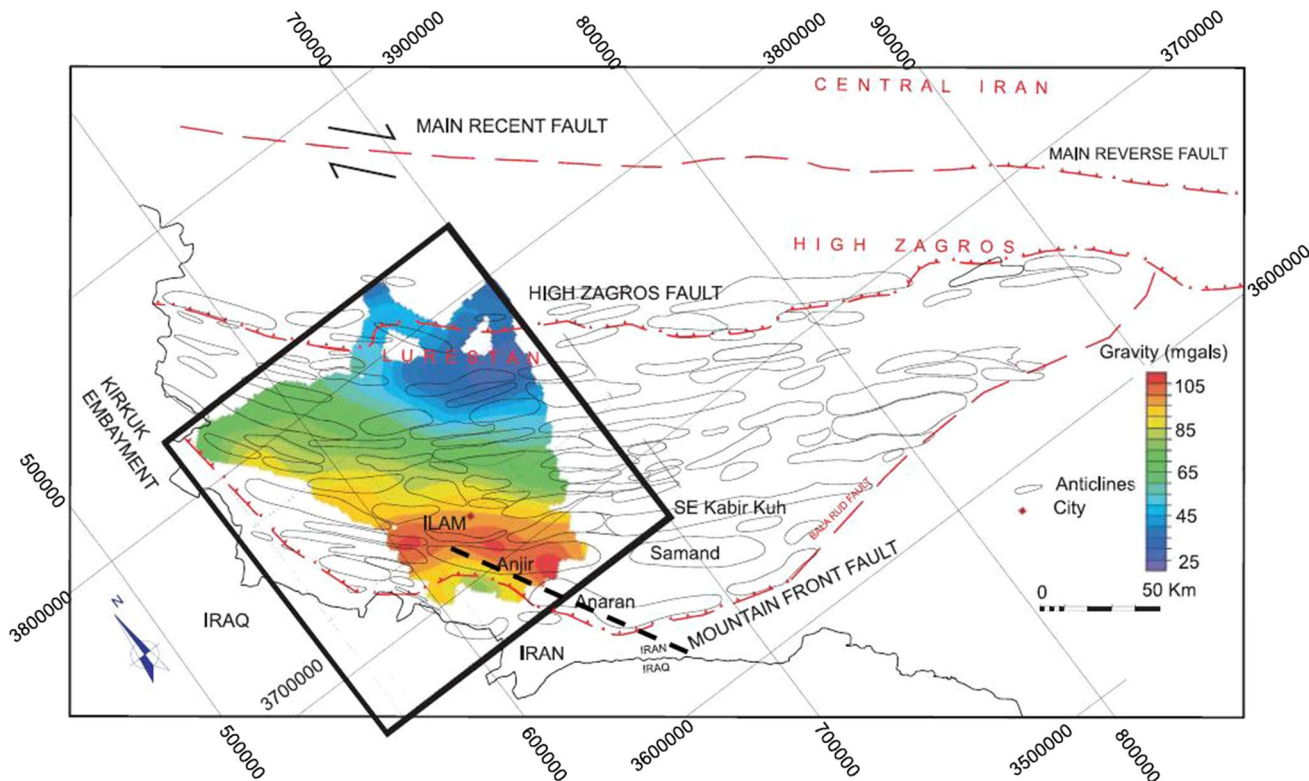


Fig. 4 Bouguer anomaly map of the study area with a 20-km low-pass filter. The map shows thickening of the sedimentary cover in the Lurestan foreland basin. Dashed lines indicate the approximately

north–south trending Anaran Basement Fault (modified after Farzipour-Saein et al. 2009a)

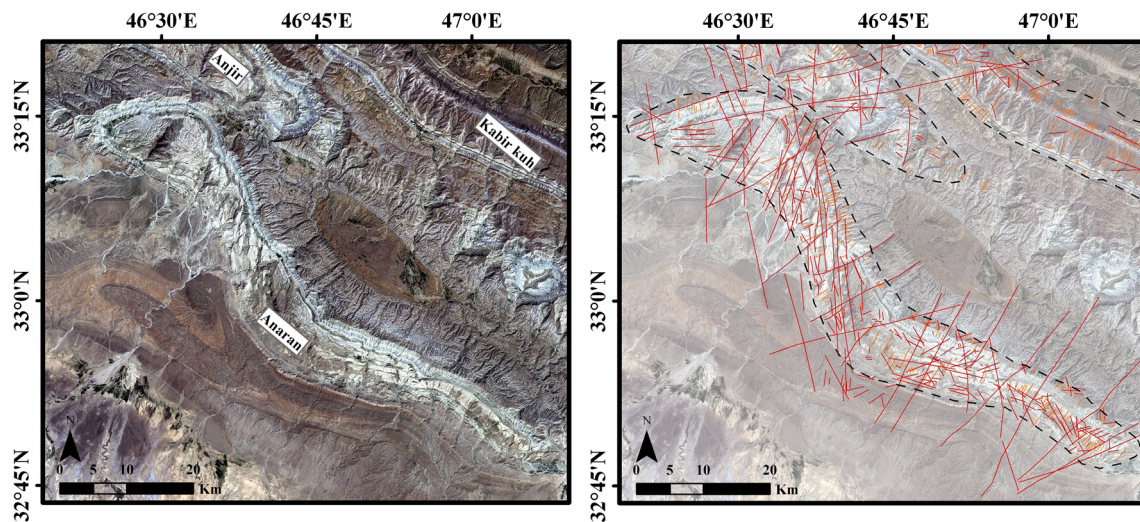


Fig. 5 Landsat (ETM⁺) image (*left*) and lineament interpretation (*right*) over the Anaran anticline (see location in Fig. 2a). The *black dashed line* marks outline of the anticline, the *red lines* show struc-

tural fractures, and the *orange line* shows lineaments, which could be structural or drainage

basement structures have been studied by different methods (Emami et al. 2010; Snidero et al. 2011; Tavani et al. 2014). Emami et al. (2010) studied the temporal evolution of the Anaran anticline by using a series of analogue models and field observations. They believed that the Mountain Front Flexure has influenced the evolution of the Anaran anticline. However, the effect of transverse basement faults on the Anaran anticline evolution was poorly considered in their studies, whereas the role of transverse basement faults in evolution of surface structures has already been confirmed by other researchers (Berberian 1995; Hessami et al. 2001a, b; Sepehr and Cosgrove 2005; Farzipour-Saein et al. 2009a, 2013; Allen and Talebian 2011). Moreover, Snidero et al. (2011) used remote sensing method to demonstrate the Anaran surface structures and their relationships to deeper structures in the basement. The geometry of the upper Cretaceous and Oligocene–Miocene sedimentary layers and also geometry of the anticline, allow structural interpretation of deeper structures (Farzipour-Saein et al. 2009a).

Methodology

In this study, we used satellite images, published geological maps (1:100,000 and 1:250,000 published by National Iranian Oil Company) and field data to establish geometric and kinematic relationships of fractures of the study area. Spatial distribution, orientation and size of fractures were analyzed using ArcGIS 10, ER Mapper 7, Global Mapper 15 and Rockwork softwares. The Landsat 7 images, Enhanced Thematic Mapper plus (ETM⁺), with 30-m

spatial resolution and Shuttle Radar Topography Mission (SRTM) data were used in our analysis. After initial image analysis, the fractures were identified and spatial data of the linear features were stored as line shape files in Geographic Information System (GIS) database. To investigate the local development of fractures and fracture pattern changes, the study area was divided into five zones. Each zone located in certain distance from the ABF zone. Moreover, in order to demonstrate the variation of fracture orientations, two statistical parameters, e.g., circular mean value and circular standard deviation, were estimated using Polar plots program (Jenness 2014). Rose diagrams for different fracture systems in different zones were plotted and compared to each other. The fractures obtained from remote sensing analysis were correlated to field observations.

Results

Fractures in the study area were analyzed for the Anaran, Anjir, Kabir Kuh, Surgah, Ilam and two unnamed anticlines (hereafter called as A1 and A2 folds; Figs. 5, 6, 7a). In zones 1, 3 and 5 (Fig. 7), the NE–SW fractures are dominant. Also, some fracture sets (E–W, N–S and NW–SE) are visible in zones 1 and 3, but they are scarce in zone 5. The zones 2 and 4 are exactly located above the ABF zone (Fig. 7a). In these sectors, the N–S and NE–SW fractures are dominant and some fractures with NNW trend exist (Fig. 7d, f).

Fractures within the study area can be categorized into two general types: intra-fold and trans-fold fractures. An intra-fold fracture is a member of a set of fold-related

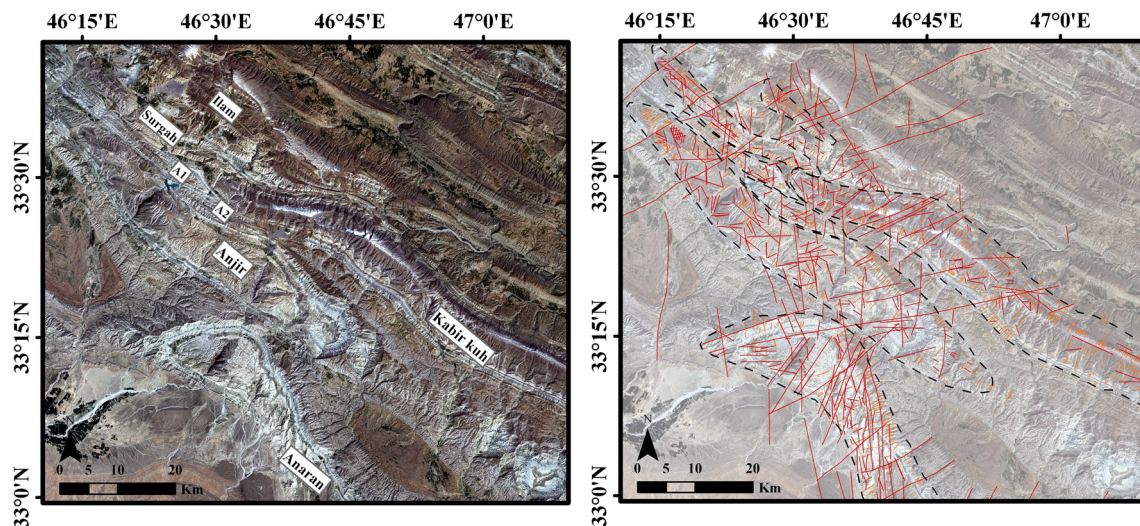


Fig. 6 Landsat (ETM⁺) image (*left*) and lineament interpretation (*right*) over the Anjir, Kabir Kuh, Surgah, Ilam, A1 and A2 anticlines (see location in Fig. 2a). The *black dashed line* marks outline of the

anticline, the *red lines* show structural fractures, and the *orange line* shows lineaments, which could be structural or drainage

fractures and is confined to the interior of a fold polygon (Stephenson et al. 2007). A trans-fold fracture is a member of a set of fractures that transect (cuts across) one or several folds polygons (Stephenson et al. 2007; Mobasher and Babaie 2008). Although trans-fold fractures transect fold polygon, in general, some fractures of a trans-fold fracture set may have small size and existed in a fold polygon (because of its small size), however, all members of an intra-fold fracture set are limited by fold polygon. In the study area, intra-fold fractures include several sets of fractures and their orientations have been presented by a rose diagram (Fig. 8a). Since the axial traces of some folds have been changed from general trend of the ZFTB in the study area, fold-associated fractures have formed in various orientations. In this case, there are dozens of fracture sets that make statistical analysis of fractures complicated and meaningless. For this reason, intra-fold fractures were interpreted only in NW–SE trending parts of the anticlines. Therefore, intra-fold fractures include the NE–SW fracture set with the mean direction of N45°, the NW–SE fracture set with the mean direction of about N125° and two small sets of fractures with approximately N–S and E–W trends (Fig. 8b).

Orientations of all trans-fold fractures throughout the study area are presented in Fig. 8c. These fractures were not limited to a special part of an anticline and were considered from its all parts. Trans-fold fractures include: N–S trending fractures, NE–SW fracture set with the mean direction of N60°, and two sets of NW–SE trending fractures with the mean directions of about N150° and N165° (Fig. 8c).

Discussion

Two major fracture systems in fold–thrust belts are fault- and fold-related fractures (Twiss and Moores 1992; Cooper et al. 2006; Stephenson et al. 2007; Mobasher and Babaie 2008; Nemcok et al. 2009). In this study, we identified numerous fracture sets that can belong to pre-, syn- or post-folding events and can be distinguished by detailed geometrical and chronological studies (Ahmadhadi et al. 2007; Lacombe et al. 2011; Chu et al. 2013). In this study, using remote sensing techniques and field controls, these fracture sets were grouped distinctly either relative to the structural elements of folds or to the preexisting basement fault throughout the study area. Those fractures that were less systematic and less abundant than the other analyzed fractures were not considered in our analyses.

An intra-fold fracture has a well-defined geometrical relationship to the confining fold elements and may belong to the axial, cross-axial and oblique fractures (Stephenson et al. 2007; Mobasher and Babaie 2008). The axial extensional set is formed parallel to the fold axis; a cross-axial extensional set is formed perpendicular to the fold axis, and two sets of conjugate shear fractures are oblique to the fold axis with their obtuse angle intersecting the trend of the fold axis (Stearns and Friedman 1972). In unchanged parts of the folds (out of the ABF shear zone), the intra-fold fractures (i.e., fold-related fractures) demonstrate a good relation to structural elements of folds (Fig. 9). Thus, the NW–SE trending intra-fold fractures which are comparable with general trend of folds in the ZFTB could be considered as fold-related axial fractures (Figs. 9, 10a, b). Moreover, the

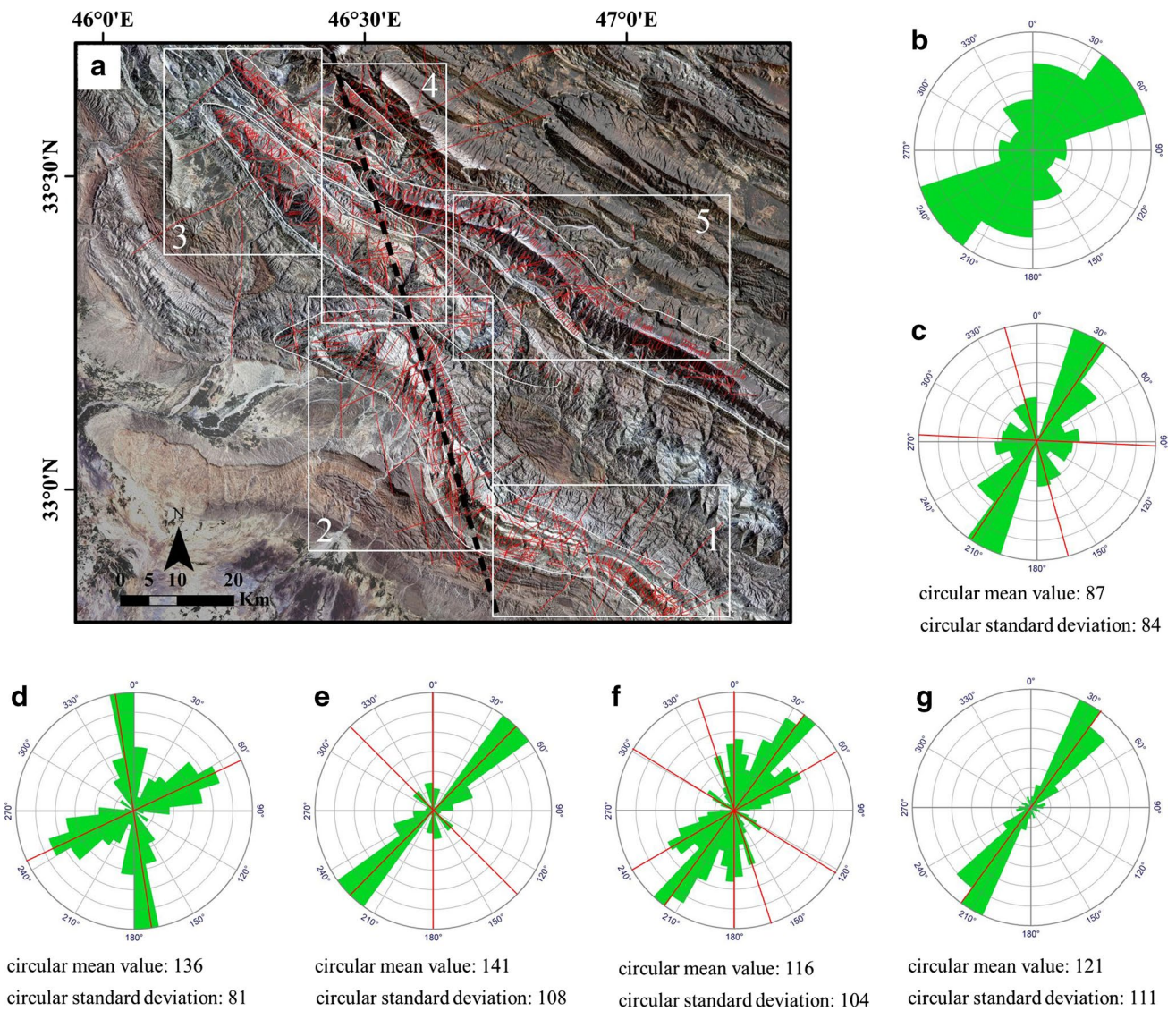


Fig. 7 **a** Satellite image (ETM⁺ draped over SRTM topography) of the study area superimposed by all fractures above the anticlines (ABF is marked by dashed line). The rectangles show five different zones used in our fracture analysis. Rose diagrams showing the strikes of fractures of **b** all fractures throughout the study area, **c** zone

1, **d** zone 2, **e** zone 3, **f** zone 4 and **g** zone 5. Mean direction of each set is marked by red line, and two statistical parameters, e.g., circular mean value and circular standard deviation, are presented for each zone

NE–SW trending intra-fold fractures with mean direction of N045°, which are perpendicular to the fold axes, could be considered as fold-related cross-axial fractures (Figs. 9, 10a). Two sets of approximately N–S trending and E–W trending fractures have lower frequency and could be considered as fold-related conjugate oblique fractures (Figs. 9, 11). As mentioned before, there are some folds that their axes have been deflected from the general NW–SE trend of the ZFTB. The Anaran, Kabir Kuh and Surgah folds demonstrate a clear sinuosity in their different parts (Figs. 2, 7a). These deflections obviously change the orientation of their belonged fold-related fractures (Figs. 7, 10, 11).

Most of the basement faults in the Zagros are buried (Berberian 1995); therefore, determination of their location and orientation needs more data and analysis. For example, subsurface data, earthquake locations and mechanisms and fracture analysis can be used to infer the characteristics of these basement faults (Berberian 1995; Hessami et al. 2001a; Bahroudi and Talbot 2003; Sepehr and Cosgrove 2005; Mobasher and Babaie 2008; Farzipour-Saein et al. 2009a, 2013; Nilfouroushan et al. 2013). Our fracture analysis, based on remote sensing and field observations, shows that excluding the fold-related fractures, the rest of the fractures (i.e., trans-fold fractures) can be categorized in four

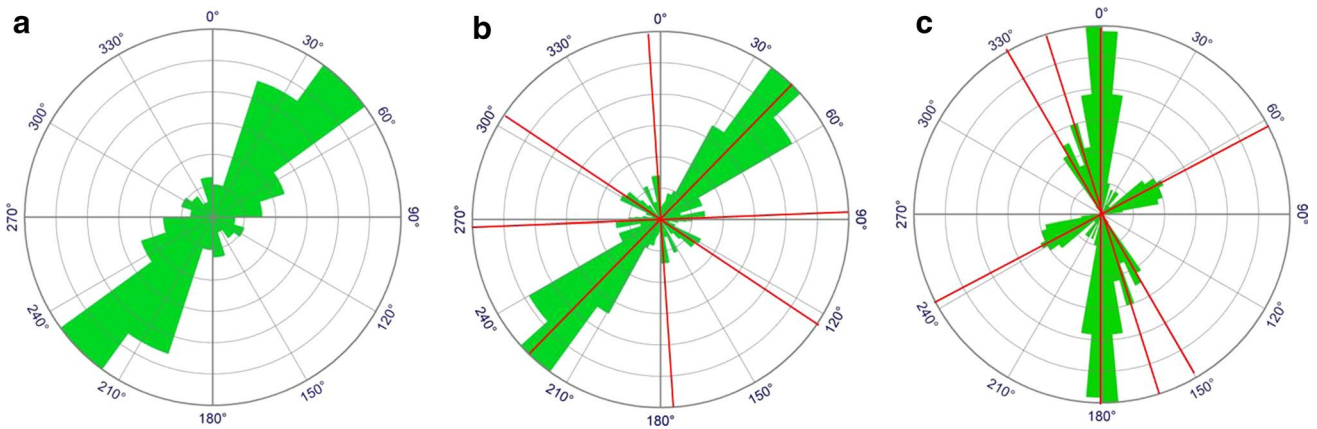
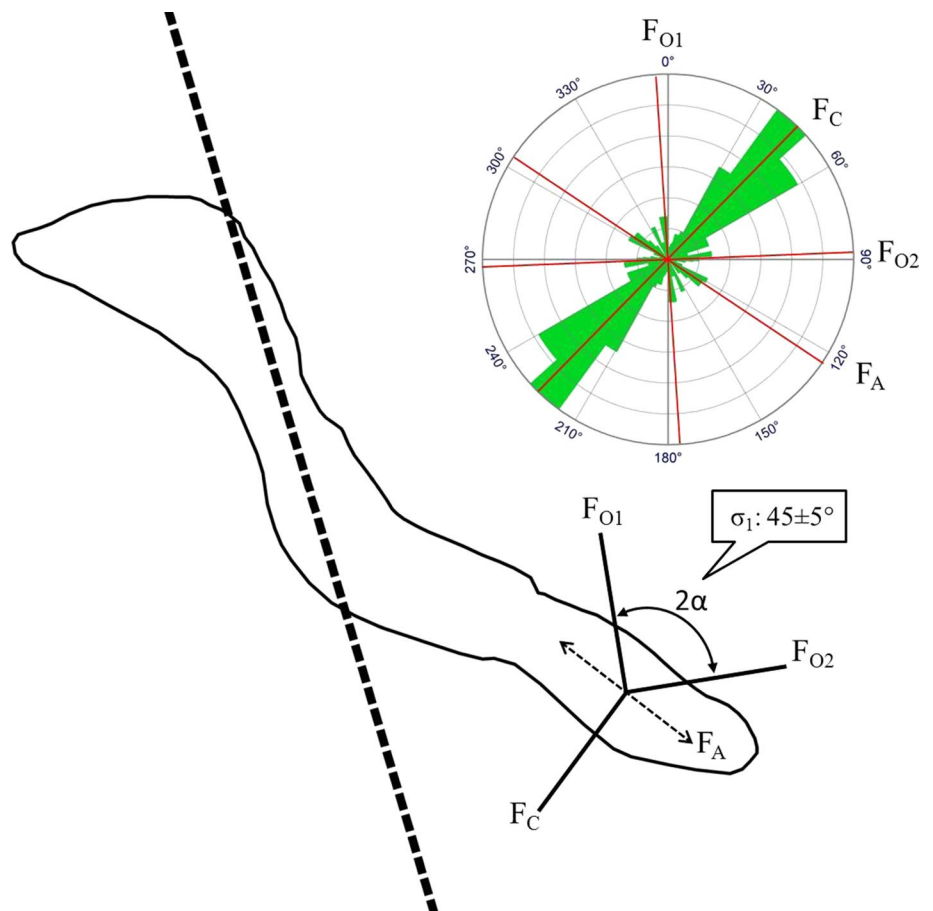


Fig. 8 Rose diagrams showing the direction of **a** the all intra-fold fractures, **b** the intra-fold fractures in unchanged parts of the folds, where the fold axes are not rotated, **c** the all trans-fold fractures. Mean direction of each set is marked by *red line*

Fig. 9 Schematic illustration shows the location of the fold-related fracture sets axial (F_A), cross-axial (F_C), and the two oblique sets (F_{O1} and F_{O2}) associated with Anaran fold (in southern part of the fold which is unrotated), and location of the ABF is marked by *dashed line*. The bisector of angle 2α , i.e., bisector of two fold-related oblique sets that are approximately parallel to the cross-axial fractures. Rose diagram showing the *strikes* of fold-related fractures in unchanged parts of the folds. The mean maximum principal compressive stress direction (σ_1) calculated from these sets of fractures



sets based on their directions (Fig. 8c), i.e., N–S trending (mean direction of $N00^\circ \pm 5^\circ$), NE–SW trending (mean direction of $N60^\circ$) and two sets of NW–SE trending fractures (mean directions of $N150^\circ$ and $N165^\circ$). These trans-fold fracture sets are main regional trends across the study area and visible in all anticlines, no matter different orientation of their axes. They have no relation to the structural

grain of the folds; thus, the origin of these fracture sets is not related to folding. Numerous N–S and NE–SW trending lineaments have cut the Anaran anticline (Fig. 5). Orientations and right-lateral shear sense of N–S trending fractures were confirmed by field observations (Fig. 12) and are clearly visible in satellite images (Figs. 5, 6). Based on the spatial distribution and orientations of these lineaments, we

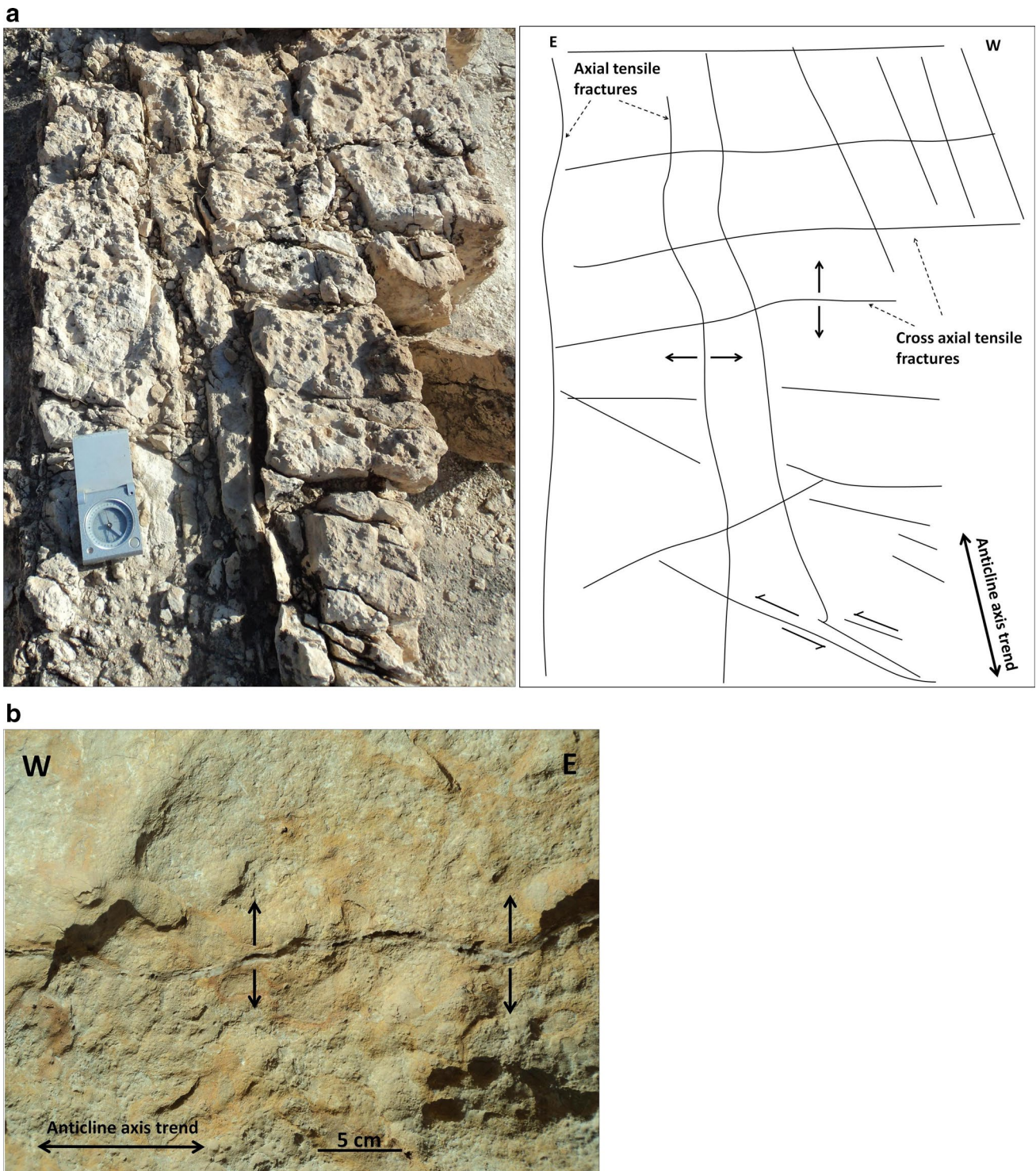


Fig. 10 Fracture patterns observed in the Anaran anticline (see location in Fig. 2a), **a** field sample and line drawing showing the main fold-related fracture sets in the Asmari Fm. In this part of the Anaran

anticline, the fold axis has been changed from original NW–SE trend to approximately N–S trend. **b** Example of axial tensile fractures in the carbonate series of Sarvak Fm

suggest their association with reactivation of deep-seated preexisting basement fault, in the basement or the overlying overburden. The geometrical relationship between these

sets and their shear sense demonstrates the assemblage of the Riedel shear fractures. Fault-related fractures are different sets which develop at a special angle to main fault

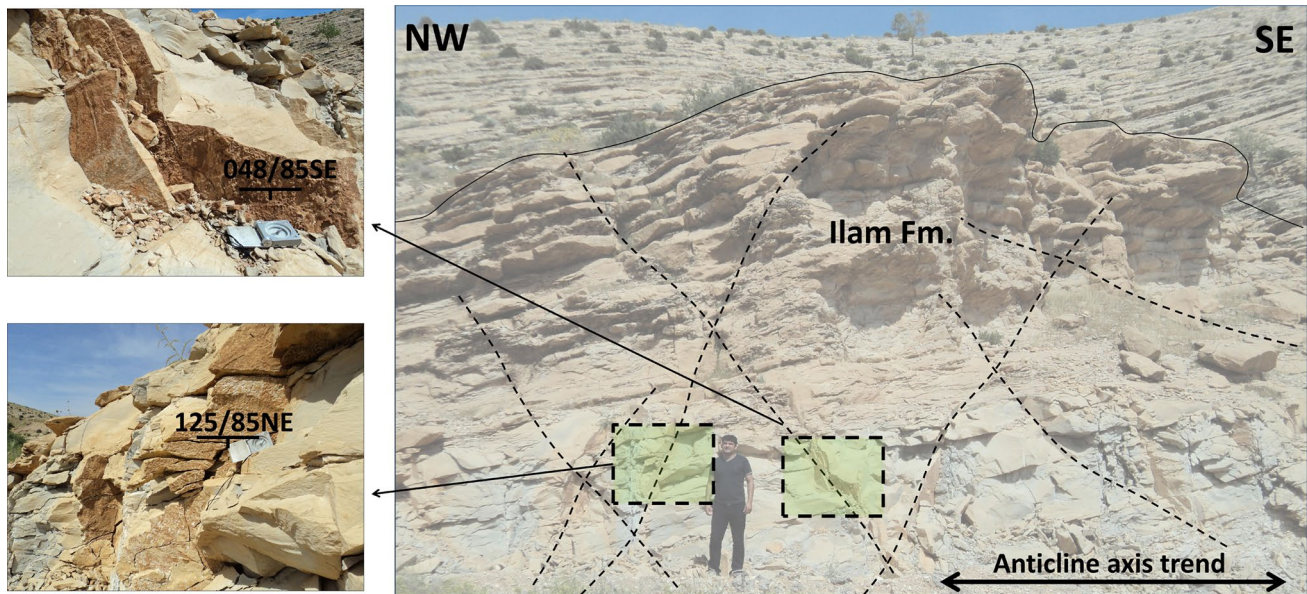


Fig. 11 Example of the conjugate oblique shear fractures observed in the field (see location in Fig. 2a), and in this part of the Anaran anticline, the fold axis has been deflected from original NW–SE trend

(Price 1966; McClay 1987; Twiss and Moores 1992; Wibberley et al. 2008; Mukherjee 2013a, b, 2014; Misra et al. 2014, 2015), and also, the existence of the N–S trending ABF has been documented well (Player et al. 1966; Farzipour-Saein et al. 2009a). Having the orientation of these four sets and also the shear sense of each set, we categorized them to R ($N00^\circ \pm 5^\circ$), R' ($N60^\circ$), P ($N150^\circ$) and Y ($N165^\circ$) fracture sets (Fig. 13). The R, P and Y fracture sets are dextral, and R' fracture set is sinistral (Figs. 12, 13). It can be seen that the strike of the Y shear fractures is close to the ABF trend and has been assumed to be parallel to main fault (Fig. 13) and R and P shear fractures develop at small angle ($15^\circ \pm 5^\circ$ CW and CCW, respectively) to main fault (McClay 1987; Mukherjee and Koyi 2010). Therefore, these fractures were considered as N–S trending ABF-related shear fractures. The ABF-related fractures (Figs. 12, 13) also support the dextral sense of the ABF. It appears that the surface structures in the study area are possibly affected by a significant right-lateral shear, probably imposed by a deep-seated basement fault. The right-lateral movement across the Anaran anticline was also confirmed by Tavani et al. (2014). Moreover, the Tigris River demonstrates a great dextral movement and its route has changed (Fig. 1). It seems that, this river channel is controlled by right-lateral shear of the ABF.

There are numerous N–S trending normal faults (with strike-slip component) cutting the Anaran anticline reported in previous studies (Emami et al. 2010; Casini et al. 2011). These faults are also visible in the satellite images (Fig. 5). The extensional faulting in the area was

suggested to be associated with the erosional uplift of the crestal sector of the Anaran anticline, before or during the early stages of folding (Tavani et al. 2014). It is noteworthy that the ABF has been active as paleohigh in Cenomanian and Oligocene–Miocene intervals (Farzipour-Saein et al. 2009a). Thus, the orientations of these normal faults are approximately parallel to the ABF and could be surface expression of the Anaran Paleohigh which could be formed by the ABF reactivation.

The bisector azimuth of the two fold-related oblique fracture sets is approximately sub-parallel to the mean orientation of the cross-axial set (McClay 1987; Twiss and Moores 1992). This implies that the fold-related cross-axial fractures are extensional fractures (as the bisector of the two oblique shear fracture sets) and probably have been formed sub-parallel to the maximum principal compressive stress (σ_1). Direction of the maximum principal compressive stress (σ_1) has been measured from bisector azimuth of the two oblique shear fracture sets and the direction of cross-axial fracture set (in unrotated parts of folds axes), which is $N45^\circ \pm 5^\circ$ (Fig. 9). The geometrical relationships between these fractures (fold-related fractures) and fold elements (axial trace) indicate that the compressional stress direction (inferred from σ_1) that formed the folds, also formed the fractures synchronously (Price 1966; Friedman 1969; Stearns and Friedman 1972; Pollard and Aydin 1988; Mobasher and Babaie 2008). Therefore, in our study area, the fold-related fractures are good indicators for fold kinematics, where the axes of the folds are not rotated in outside of the ABF shear zone. Although strike-slip faults may cause stress

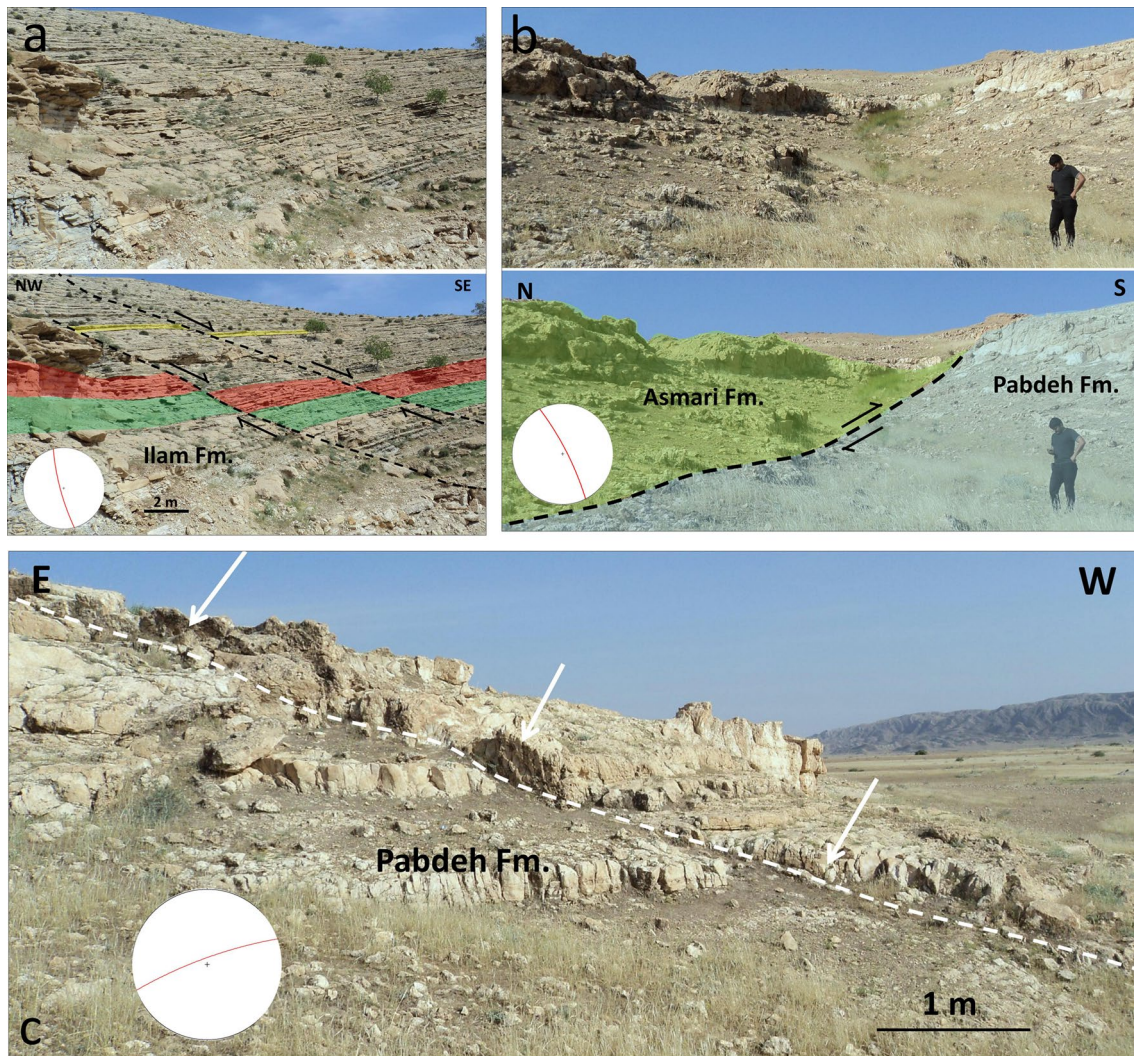


Fig. 12 Example of the fault-related fractures observed in the field (see locations in Fig. 2a), **a** Carbonate series of the Ilam Fm. in NW flank of the Anaran anticline, shows the approximately north–south trending strike-slip fault with right-lateral shear sense (the stereogram of faults has been *plotted*). **b** Examples of the strike-slip faults within the forelimb of the Anaran anticline, the Pabdeh Fm. has located

adjacent to the Asmari Fm. by right-lateral movement of the strike-slip fault (the stereogram of fault has been *plotted*). **c** Example of the strike-slip fault in NW flank of the Anaran anticline, shown by *dashed line*. This fault is sinistral and parallel to R' fracture sets (the stereogram of fault has been *plotted*)

perturbations (Homberg et al. 1997, 2004), kinematic analysis has been carried out by studying fault-related fracture sets (Riedel fractures) within different fault shear zones (Mandl 1988; Mobasher and Babaie 2008). Mean compressional stress direction (σ_1) determined from orientation of the Riedel shear fractures (bisector of the angle between R and R') in the ABF zone, is $N30^\circ \pm 5^\circ$ (Fig. 13). This azimuth of compressional stress resulted from our analysis is close to the value (σ_1) deduced from analyses of earthquake and geodetic data (Zarifi et al. 2014).

Casini et al. (2011) carried out a fracture study in the Lurestan region. They presented a model for timing of fractures in the anticlines of the Lurestan region (e.g., Anaran

and Siah Kuh anticlines) and believe that strike-slip fault system is probably related to late stages of fold tightening (or after folding). They also concluded that N–NE shortening direction is related to the strike-slip faults in the area. This shortening direction is similar to our results from the ABF-related fracture analysis. However, our results demonstrate that, the mean shortening direction determined from the fault-related fractures in the ABF shear zone (Fig. 13) is different from the orientation of shortening calculated from the fold-related fracture sets (Fig. 9), outside of the ABF shear zone. This difference probably indicates formation of the fractures in different two stages of deformation throughout the area.

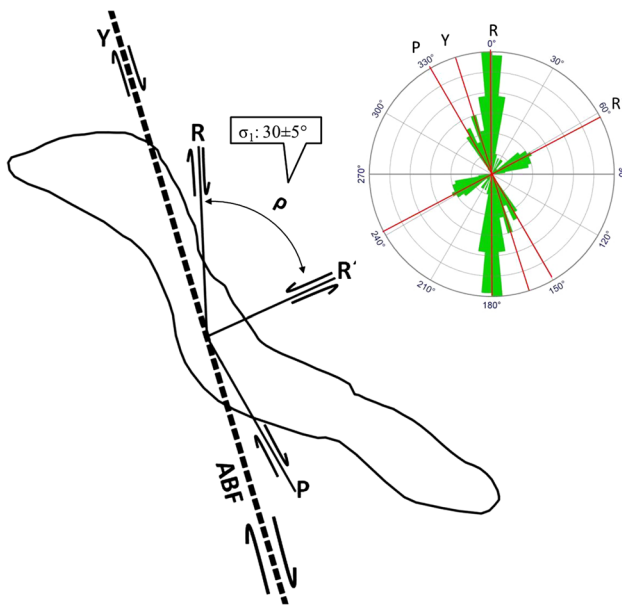


Fig. 13 Diagram illustrating angular relationships between the right-lateral *ABF* and the following fault-related fracture sets (*R*, *R'*, *P* and *Y*). Rose diagram showing the strikes of regional trans-fold fractures (i.e., *ABF*-related fractures). The mean maximum principal compressive stress direction (σ_1) calculated from bisector of the mean direction of *R* and *R'* fracture sets

In the study area, the Anaran, Kabir Kuh, Ilam and Surgah folds demonstrate a clear sinuosity in their different parts (Figs. 1, 7a). Measuring deviation angle of the fold axis within the *ABF* shear zone compared to direction of the fold axis outside the *ABF* shear zone can determine the angle and rotation sense (CW vs. CCW) of the folds (Mobasher and Babaie 2008; Fig. 14). The rotation angles (β) of the Ilam, Anjir and A1 anticlines are 30°, 20° and 22° (CW), respectively. The Kabir Kuh anticline, one of the largest anticlines in the ZFTB, demonstrates $15^\circ \pm 1^\circ$ (CW) of rotation angle in its NW nose compared to its original NW–SE trend in its other parts. The Anaran anticline shows maximum amount of rotation angle compared to other anticlines. In central part of the Anaran anticline, the fold axis of this anticline is rotated from its original NW–SE trend to approximately north–south trend by about 35° CW (Fig. 14). In the Fars region, the sinuosity of folds has been attributed to linkage of previous folds (Ramsey et al. 2008). Based on this scenario, Emami et al. (2010) suggested that, the sinuosity of the Anaran anticline has developed by the linkage of two anticlines. On the other hand, rotation of a single fold (e.g., caused by reactivation of the preexisting basement faults) has been proposed for sinuosity of folds (Player et al. 1966; Aubourg et al. 2008; Mobasher and Babaie 2008; Farzipour-Saein et al. 2009a, 2013). Farzipour-Saein et al. (2009a) believe that sinuosity of the Anaran anticline is related to offset on the Anaran

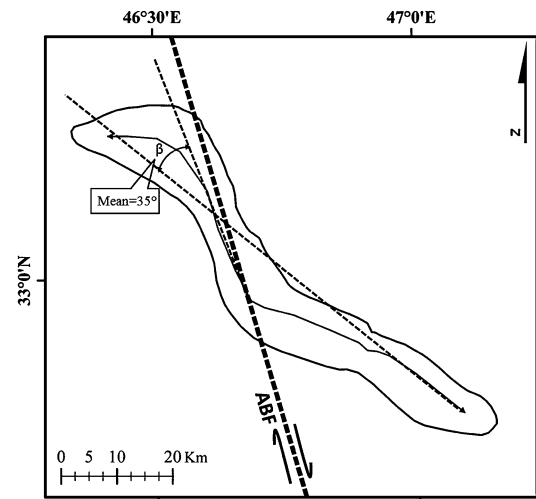


Fig. 14 Schematic illustration shows the rotation angle (β) of the fold axial trace of the Anaran anticline

lineament in the basement which can be followed into the northern flank of the Kabir Kuh anticline. The axial traces of the folds, especially the Anaran anticline, demonstrate a right-lateral offset along the *ABF*, such that, in central part of the Anaran anticline, the fold axis of this anticline is changed from its original NW–SE trend to approximately north–south trend of the *ABF* (Figs. 1, 5). We believe that whatever scenario (linkage of previous folds or rotation of a single fold) caused observed sinuosity of the folds throughout the study area, and the reactivation of the *ABF* has influenced to some degree the geometrical evolution of the anticlines in the study area. However, the degree of this coupling between Anaran basement faulting and cover deformation in this area should be investigated by further field observations and geophysical surveys.

Conclusions

During evolution of the ZFTB, architecture of the foreland basin was influenced by the deep-seated, approximately north–south trending Anaran Basement Fault (*ABF*) in the Lurestan region. Our fracture analysis shows that approaching the Anaran Basement Fault, the fracture pattern changes and the fractures association with reactivation of the deep-seated preexisting Anaran Basement Fault can be categorized in four sets based on their directions, i.e., N–S trending (mean direction of $N00^\circ \pm 5^\circ$), NE–SW trending (mean direction of $N60^\circ$) and two sets of NW–SE trending fractures (mean directions of $N150^\circ$ and $N165^\circ$). The geometrical relationship between these sets and their shear sense demonstrates the assemblage of the Riedel shear fractures. The mean direction for maximum compressional

stress is different between the fault- and fold-related fractures within and around the ABF shear zone. We estimated an orientation of $N30^\circ \pm 5^\circ$ for the fault-related fractures and $N45^\circ \pm 5^\circ$ for the fold-related fracture sets outside of the ABF shear zone. This difference suggests that the fold-related and fault-related fracture sets have been formed in different two stages of deformation throughout the area. The ABF-related fractures also support the dextral sense of the ABF. It appears that the surface structures in the study area are possibly affected by a significant right-lateral shear, probably imposed by a deep-seated basement fault.

The extensional faulting in the area was suggested to be associated with the erosional uplift of the crestal sector of the Anaran anticline, and the orientations of these normal faults are approximately parallel to the ABF and could be surface expression of the Anaran Paleohigh.

The Anaran, Kabir Kuh, Ilam and Surgah folds demonstrate a clear sinuosity in their different parts. The axial traces of the folds, especially the Anaran anticline, demonstrate a right-lateral offset along the ABF, such that, in central part of the Anaran anticline, the fold axis of this anticline is changed from its original NW–SE trend to approximately north–south trend of the ABF.

Acknowledgments The authors are very grateful to Stefano Tavani and Soumyajit Mukherjee for careful and constructive reviews, which helped us to greatly improve this manuscript. We also acknowledge Wolf-Christian Dullo and Soumyajit Mukherjee for handling our manuscript and Katayoun Mobasher who introduced us some relevant articles. Moosarrez Toori is thanked for his help with the structural transect. AFS thanks the research and postgraduate office in University of Isfahan for their support. FN was funded by Swedish Research Council (VR).

References

- Agard P et al (2011) Zagros orogeny: a subduction-dominated process. *Geol Mag* 148:692–725
- Ahmadhadi F, Lacombe O, Daniel J-M (2007) Early reactivation of basement faults in Central Zagros (SW Iran): evidence from pre-folding fracture populations in Asmari Formation and lower Tertiary paleogeography. In: Thrust belts and foreland basins. Springer, Berlin, pp 205–228
- Ahmadhadi F, Daniel JM, Azzizadeh M, Lacombe O (2008) Evidence for pre-folding vein development in the Oligo–Miocene Asmari Formation in the Central Zagros Fold Belt, Iran. *Tectonics*. doi:10.1029/2006TC001978
- Alavi M (2007) Structures of the Zagros fold–thrust belt in Iran. *Am J Sci* 307:1064–1095
- Allen MB (2010) Roles of strike-slip faults during continental deformation: examples from the active Arabia–Eurasia collision. *Geol Soc Lond Spec Publ* 338:329–344
- Allen MB, Talebian M (2011) Structural variation along the Zagros and the nature of the Dezful Embayment. *Geol Mag* 148:911–924. doi:10.1017/S0016756811000318
- Amrouch K, Lacombe O, Bellahsen N, Daniel JM, Callot JP (2010) Stress and strain patterns, kinematics and deformation mechanisms in a basement-cored anticline: Sheep Mountain Anticline, Wyoming. *Tectonics* 29(TC1005):1–27. doi:10.1029/2009TC002525
- Anastasio DJ, Fisher DM, Messina TA, Holl JE (1997) Kinematics of décollement folding in the Lost River Range, Idaho. *J Struct Geol* 19:355–368
- Aubourg C, Smith B, Bakhtari H, Guya N, Eshraghi A (2008) Tertiary block rotations in the Fars arc (Zagros, Iran). *Geophys J Int* 173:659–673
- Authemayou C, Chardon D, Bellier O, Malekzadeh Z, Shabanian E, Abbassi MR (2006) Late Cenozoic partitioning of oblique plate convergence in the Zagros fold-and-thrust belt (Iran). *Tectonics* 25(TC3002):1–21. doi:10.1029/2005TC001860
- Bahroudi A, Koyi H (2003) Effect of spatial distribution of Hormuz salt on deformation style in the Zagros fold and thrust belt: an analogue modelling approach. *J Geol Soc* 160:719–733
- Bahroudi A, Koyi HA (2004) Tectono-sedimentary framework of the Gachsaran Formation in the Zagros foreland basin. *Mar Pet Geol* 21:1295–1310
- Bahroudi A, Talbot C (2003) The configuration of the basement beneath the Zagros basin. *J Pet Geol* 26:257–282
- Baker C, Jackson J, Priestley K (1993) Earthquakes on the Kazerun line in the Zagros Mountains of Iran: strike-slip faulting within a fold-and-thrust belt. *Geophys J Int* 115:41–61
- Bellahsen N, Fiore P, Pollard DD (2006) The role of fractures in the structural interpretation of Sheep Mountain Anticline, Wyoming. *J Struct Geol* 28:850–867
- Berberian M (1995) Master “blind” thrust faults hidden under the Zagros folds: active basement tectonics and surface morphotectonics. *Tectonophysics* 241:193–224
- Berberian M, King G (1981) Towards a paleogeography and tectonic evolution of Iran. *Can J Earth Sci* 18:210–265
- Blanc E-P, Allen MB, Inger S, Hassani H (2003) Structural styles in the Zagros simple folded zone, Iran. *J Geol Soc* 160:401–412. doi:10.1144/0016-764902-110
- Burberry CM (2015) The effect of basement fault reactivation on the Triassic–recent geology of Kurdistan, north Iraq. *J Pet Geol* 38:37–58
- Carminati E et al (2013) Control of Cambrian evaporites on fracturing in fault-related anticlines in the Zagros fold-and-thrust belt. *Int J Earth Sci* 102:1237–1255
- Casini G et al (2011) Sub-seismic fractures in foreland fold and thrust belts: insight from the Lurestan Province, Zagros Mountains, Iran. *Pet Geosci* 17:263–282. doi:10.1144/1354-079310-043
- Chu HT, Lee J-C, Bergerat F, Hu J-C, Liang S-H, Lu C-Y, Lee T-Q (2013) Fracture patterns and their relations to mountain building in a fold–thrust belt: a case study in NW Taiwan. *Bull Soc Géol Fr* 184(4–5):485–500
- Cooper SP, Goodwin LB, Lorenz JC (2006) Fracture and fault patterns associated with basement-cored anticlines: the example of Teapot Dome, Wyoming. *AAPG Bull* 90:1903–1920
- Emami H (2008) Foreland propagation folding and structure of the Mountain Front Flexure in the Pusht-e Kuh arc (NW Zagros, Iran), PhD thesis. Universitat de Barcelona
- Emami H et al (2010) Structure of the Mountain Front Flexure along the Anaran anticline in the Pusht-e Kuh Arc (NW Zagros, Iran): insights from sand box models. *Geol Soc Lond Spec Publ* 330:155–178
- Falcon NL (1974) Southern Iran: Zagros Mountains. *Geol Soc Lond Spec Publ* 4:199–211
- Farzipour-Saein A, Yassaghi A, Sherhati S, Koyi H (2009a) Mechanical stratigraphy and folding style of the Lurestan region in the Zagros fold–thrust belt, Iran. *J Geol Soc* 166:1101–1115
- Farzipour-Saein A, Yassaghi A, Sherhati S, Koyi H (2009b) Basin evolution of the Lurestan region in the Zagros fold-and-thrust belt, Iran. *J Pet Geol* 32:5–19

- Farzipour-Saein A, Nilfouroushan F, Koyi H (2013) The effect of basement step/topography on the geometry of the Zagros fold and thrust belt (SW Iran): an analog modeling approach. *Int J Earth Sci* 102:2117–2135
- Friedman M (1969) Structural analysis of fractures in cores from Saticoy Field, Ventura County, California. *AAPG Bull* 53:367–389
- Gholipour AM (1998) Patterns and structural positions of productive fractures in the Asmari reservoirs, Southwest Iran. *J Can Pet Technol* 37:44–50
- Hessami K, Koyi H, Talbot C (2001a) The significance of strike-slip faulting in the basement of the Zagros fold and thrust belt. *J Pet Geol* 24:5–28
- Hessami K, Koyi HA, Talbot CJ, Tabasi H, Shabanian E (2001b) Progressive unconformities within an evolving foreland fold–thrust belt, Zagros Mountains. *J Geol Soc* 158:969–981
- Homberg C, Hu J, Angelier J, Bergerat F, Lacombe O (1997) Characterization of stress perturbations near major fault zones: insights from 2-D distinct-element numerical modelling and field studies (Jura mountains). *J Struct Geol* 19:703–718
- Homberg C, Angelier J, Bergerat F, Lacombe O (2004) Using stress deflections to identify slip events in fault systems. *Earth Planet Sci Lett* 217:409–424
- Homke S, Vergés J, Garcés M, Emami H, Karpuz R (2004) Magnetostratigraphy of Miocene–Pliocene Zagros foreland deposits in the front of the Push-e Kush arc (Lurestan Province, Iran). *Earth Planet Sci Lett* 225:397–410
- Jenness J (2014) Polar plots for ArcGIS Jenness Enterprises. http://www.jennessent.com/arcgis/polar_plotshtm
- Khoshbakht F, Memarian H, Mohammadnia M (2009) Comparison of Asmari, Pabdeh and Gurpi formation's fractures, derived from image log. *J Pet Sci Eng* 67:65–74
- Khoshbakht F, Azzizadeh M, Memarian H, Nourozi G, Moallemi S (2012) Comparison of electrical image log with core in a fractured carbonate reservoir. *J Pet Sci Eng* 86:289–296
- Koyi H (1988) Experimental modeling of role of gravity and lateral shortening in Zagros mountain belt. *AAPG Bull* 72:1381–1394
- Lacombe O, Bellahsen N, Mouthereau F (2011) Fracture patterns in the Zagros Simply Folded Belt (Fars, Iran): constraints on early collisional tectonic history and role of basement faults. *Geol Mag* 148:940–963
- Mandl G (1988) *Mechanics of tectonic faulting: models and basic concepts*, vol 407. Elsevier, Amsterdam
- McClay K (1987) *The mapping of geological structures*. Geological Society of London Handbook Series. Open University Press, London
- McQuarrie N (2004) Crustal scale geometry of the Zagros fold–thrust belt, Iran. *J Struct Geol* 26:519–535
- McQuarrie N, van Hinsbergen DJ (2013) Retrodeforming the Arabia–Eurasia collision zone: age of collision versus magnitude of continental subduction. *Geology* 41:315–318. doi:10.1130/G33591.1
- McQuillan H (1973) Small-scale fracture density in Asmari Formation of southwest Iran and its relation to bed thickness and structural setting. *AAPG Bull* 57:2367–2385
- McQuillan H (1974) Fracture patterns on Kuh-e Asmari anticline, southwest Iran. *AAPG Bull* 58:236–246
- Misra AA, Bhattacharya G, Mukherjee S, Bose N (2014) Near N-S paleo-extension in the western Deccan region, India: does it link strike-slip tectonics with India–Seychelles rifting? *Int J Earth Sci* 103:1645–1680
- Misra AA, Sinha N, Mukherjee S (2015) Repeat ridge jumps and microcontinent separation: insights from NE Arabian Sea. *Mar Pet Geol* 59:406–428
- Mobasher K, Bahaie HA (2008) Kinematic significance of fold-and fault-related fracture systems in the Zagros mountains, southern Iran. *Tectonophysics* 451:156–169
- Motiei H (1994) *Stratigraphy of Zagros*. Geological Survey of Iran Publications, Tehran (**in Persian**)
- Mouthereau F, Lacombe O, Tensi J, Bellahsen N, Kargar S, Amrouch K (2007a) Mechanical constraints on the development of the Zagros Folded Belt (Fars). In: *Thrust belts and foreland basins*. Springer, Berlin, pp 247–266
- Mouthereau F, Tensi J, Bellahsen N, Lacombe O, De Boisgrollier T, Kargar S (2007b) Tertiary sequence of deformation in a thin-skinned/thick-skinned collision belt: the Zagros Folded Belt (Fars, Iran). *Tectonics* 26(TC5006):28. doi:10.1029/2007TC002098
- Mouthereau F, Lacombe O, Vergés J (2012) Building the Zagros collisional orogen: timing, strain distribution and the dynamics of Arabia/Eurasia plate convergence. *Tectonophysics* 532:27–60
- Mukherjee S (2013a) *Deformation microstructures in rocks*. Springer, Berlin
- Mukherjee S (2013b) Higher Himalaya in the Bhagirathi section (NW Himalaya, India): its structures, backthrusts and extrusion mechanism by both channel flow and critical taper mechanisms. *Int J Earth Sci* 102:1851–1870
- Mukherjee S (2014) *Atlas of shear zone structures in meso-scale*. Springer, Berlin
- Mukherjee S, Koyi HA (2010) Higher Himalayan Shear Zone, Sutlej section: structural geology and extrusion mechanism by various combinations of simple shear, pure shear and channel flow in shifting modes. *Int J Earth Sci* 99:1267–1303
- Nemcok M, Schamel S, Gayer R (2009) *Thrustbelts: structural architecture, thermal regimes and petroleum systems*. Cambridge University Press, Cambridge
- Nilfouroushan F et al (2003) GPS network monitors the Arabia–Eurasia collision deformation in Iran. *J Geodesy* 77:411–422
- Nilfouroushan F, Pysklywec R, Cruden A, Koyi H (2013) Thermal-mechanical modeling of salt-based mountain belts with pre-existing basement faults: application to the Zagros fold and thrust belt, southwest Iran. *Tectonics* 32:1212–1226
- Player RA, Hulstrand RF, Ghashghaie M (1966) *The central Lurestan geological survey 1963–1964 IOOC Report*, No. 1103 (**Unpublished**)
- Pollard DD, Aydin A (1988) Progress in understanding jointing over the past century. *Geol Soc Am Bull* 100:1181–1204
- Price NJ (1966) *Fault and joint development in brittle and semi-brittle rock*, vol 1. Pergamon Press, Oxford
- Ramsey LA, Walker RT, Jackson J (2008) Fold evolution and drainage development in the Zagros mountains of Fars province, SE Iran. *Basin Res* 20:23–48
- Sepehr M, Cosgrove J (2004) Structural framework of the Zagros fold–thrust belt, Iran. *Mar Pet Geol* 21:829–843
- Sepehr M, Cosgrove J (2005) Role of the Kazerun Fault Zone in the formation and deformation of the Zagros Fold–Thrust Belt, Iran. *Tectonics* 24(TC5005):13. doi:10.1029/2004TC001725
- Sharp I et al (2010) Stratigraphic architecture and fracture-controlled dolomitization of the Cretaceous Khami and Bangestan groups: an outcrop case study, Zagros Mountains, Iran. *Geol Soc Lond Spec Publ* 329:343–396
- Sherkati S, Letouzey J (2004) Variation of structural style and basin evolution in the central Zagros (Izeh zone and Dezful Embayment), Iran. *Mar Pet Geol* 21:535–554
- Snidero M, Amilibia A, Gratacos O, Blanc E-P, Muñoz J (2011) The 3D reconstruction of geological structures based on remote sensing data: example from the Anaran anticline, Lurestan province, Zagros fold and thrust belt, Iran. *J Geol Soc* 168:769–782. doi:10.1144/0016-76492010-107
- Stearns DW, Friedman M (1972) *Reservoirs in fractured rock: geologic exploration methods: the American Association of Petroleum Geologists reprinted from American Association of*

- Petroleum Geologists Memoir Stratigraphic Oil and Gas Fields 16:82–106
- Stephenson BJ, Koopman A, Hillgartner H, McQuillan H, Bourne S, Noad JJ, Rawnsley K (2007) Structural and stratigraphic controls on fold-related fracturing in the Zagros Mountains, Iran: implications for reservoir development. *Geol Soc Lond Spec Publ* 270:1–21
- Stocklin J (1968) Structural history and tectonics of Iran: a review. *AAPG Bull* 52:1229–1258
- Stöcklin J (1974) Possible ancient continental margins in Iran. In: *The geology of continental margins*. Springer, Berlin, pp 873–887
- Storti F, Salvini F (2001) The evolution of a model trap in the central Apennines, Italy: fracture patterns, fault reactivation and development of cataclastic rocks in carbonates at the Narni Anticline. *J Pet Geol* 24:171–190
- Takin M (1972) Iranian geology and continental drift in the Middle East. *Nature* 235:147–150
- Talbot C, Alavi M (1996) The past of a future syntaxis across the Zagros. *Geol Soc Lond Spec Publ* 100:89–109. doi:[10.1144/GSL.SP.1996.100.01.08.1](https://doi.org/10.1144/GSL.SP.1996.100.01.08.1)
- Tavani S, Storti F, Fernández O, Muñoz J, Salvini F (2006) 3-D deformation pattern analysis and evolution of the Añisclo anticline, southern Pyrenees. *J Struct Geol* 28:695–712
- Tavani S, Storti F, Soleimany B, Fallah M, Munoz JA, Gambini R (2011) Geometry, kinematics and fracture pattern of the Bangestan anticline, Zagros, SW Iran. *Geol Mag* 148:964–979
- Tavani S, Snidero M, Muñoz J (2014) Uplift-induced residual strain release and late-thrusting extension in the Anaran mountain front anticline, Zagros (Iran). *Tectonophysics* 636:257–269
- Tavani S, Storti F, Lacombe O, Corradetti A, Muñoz J, Mazzoli S (2015) A review of deformation pattern templates in foreland basin systems and fold-and-thrust belts: implications for the state of stress in the frontal regions of thrust wedges. *Earth Sci Rev* 141:82–104
- Twiss RJ, Moores E (1992) *Structural geology*. WH Freeman, New York
- Vergés J, Goodarzi M, Emami H, Karpuz R, Efstathiou J, Gillespie P (2011) Multiple detachment folding in Pusht-e Kuh arc, Zagros: role of mechanical stratigraphy. *AAPG Memoir* 94:69–94
- Wennberg O, Svånå T, Azizzadeh M, Aqrabi A, Brockbank P, Lyslo K, Ogilvie S (2006) Fracture intensity vs. mechanical stratigraphy in platform top carbonates: the Aquitanian of the Asmari Formation, Khaviz Anticline, Zagros, SW Iran. *Pet Geosci* 12:235–246
- Wibberley CAJ, Kurz W, Imber J, Holdsworth RE, Collettini C (2008) The internal structure of fault zones: implications for mechanical and fluid-flow properties. *Geol Soc Lond Spec Publ* 299:195–210
- Zarifi Z, Nilfouroushan F, Raeesi M (2014) Crustal stress Map of Iran: insight from seismic and geodetic computations. *Pure appl Geophys* 170:1–18. doi:[10.1007/s00024-013-0711-9](https://doi.org/10.1007/s00024-013-0711-9)